Estimation of the Position and Orientation of a Planar Surface Using Multiple Beams

Jaekyu Ha and Robert M. Haralick

Intelligent Systems Laboratory
Dept. of Electrical Engineering, FT-10
University of Washington
Seattle, Washington 98195
April 6, 1992

ABSTRACT

Our aim in this paper is to estimate the surface constants of a planar work surface by using several laser beams or similar light sources. The estimation is possible when we know the beam positions and directions as well as the images of beam spots on the planar work surface. The more beams we use, the smaller will be the estimation error. However, the number of beams we can utilize, in practice, is limited in our application though our theoretical anaysis treats the general case. Clearly, the estimation errors will increase if the beam directions are arbitrary. Therefore, we need to find a certain beam pattern that can give the smallest estimation error. This will be discussed in this paper.

1. Introduction

Robots are often introduced into production to solve particular problems associated with labor practices or unreliability. However, robot operation takes place in an envirionment with numerous irregularities. Positions of manipulated objects, and corresponding manipulator configurations, often cannot be determined accurately in advance. Assessment of all possible irregularities is an extremely tedious job, but the appearance of an irregularity can result in damage and significant production delay. Therefore, it is preferable to have a robot which operates by taking into account changes in its environment, using its sensory system. This paper suggests a sensory system designed for estimating the surface constants of a planar work surface with respect to the camera attached to the end of the robot arm.

Our sensory system consists of several laser beam projectors and a camera (Fig 1) and the combination of them is called the SHEE (Sensor Head End Effector).

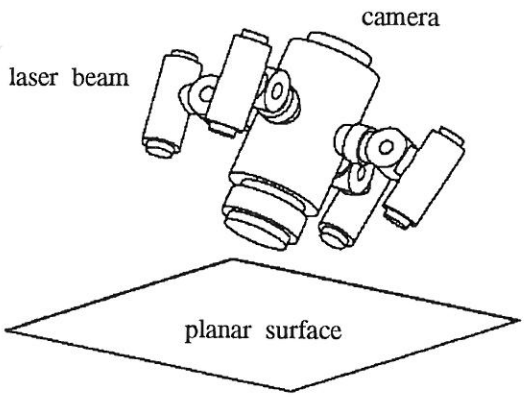

Fig 1. Sensor Head End Effector

Of course, the number of beam sources to be used for the estimation should be equal to or greater than three. When these projectors project beams onto a planar surface, we can obtain an image of the beam spots appearing on the planar work surface. Now suppose that we know the positions of the beam projectors and their projection directions. Then we can determine how much the camera is tilted with respect to the planar surface, how far the camera is from the planar work surface, and how we can adjust a robot arm so that we achieve the parallelism of the optical axis of the camera.

As an example of industrial applications, the robot equipped with SHEE can be used to paint complex surfaces such as wings and body segments for aircraft parts within a certain accuracy. Conventionally, paint robots are operated in "lead-through programming" technique wherein the end of the robot arm is moved to specific positions and distances over and away from the planar work surface, as required to perform a task. This "traditional" method of programming robot path splines is manual, very time consuming and error prone. Thus

the conventional process has adverse effect on operator fatigue and safety, product quality, product rejection ratios, production schedule, and paint booth availability time. The new technique presented in this paper will cover all these disadvantages because on-line processing is possible if a computer is used to process the images captured by a CCD camera.

Fig 2 shows various image patterns, for which four parallel beam projectors are used. A particular image pattern seems to be associated with a particular position of a planar surface. So one might think that such image patterns can be used as templates to estimate the poses of planar surfaces. However, such an approach is not preferrable. The above mentioned one-to-one correspondence holds true only in noiseless case. Even when noise is negligible, an enormous number of templates must be test matched against an image to account for possible changes in rotation and magnification of templates. Of course, it is nearly impoosible to predict uncertainties contained in the results of this approach. For these reasons, our problem will be treated analytically in this paper.

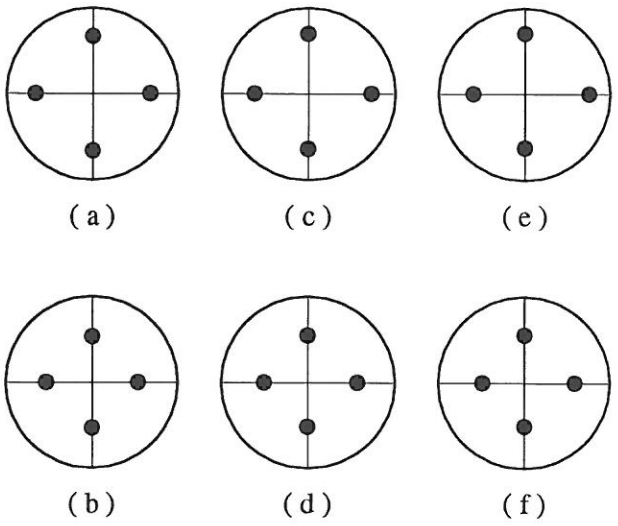

Fig 2. Image patterns of four beam spots on the plane $x\sin\theta\cos\phi + y\sin\theta\sin\phi + z\cos\theta - d = 0$ where $d > 0$. Four beams are located at $(a,0,0)$, $(0,a,0)$, $(-a,0,0)$, $(0,-a,0)$, respectively, where $a = 35$: (a) $\theta = 0°$, $d = 200$ (b) $\theta = 0°$, $d = 250$ (c) $\theta = 30°$, $\phi = 30°$, $d = 200$ (d) $\theta = 30°$, $\phi = 30°$, $d = 250$ (e) $\theta = 45°$, $\phi = 30°$, $d = 200$ (f) $\theta = 45°$, $\phi = 30°$, $d = 250$

This paper is divided into four parts: estimation, calibration, image processing, error propagation analysis, and simulation. The estimation part provides the theoretical basis for the estimation of surface constants of a planar surface. The calibration part suggests a way how to determine the beam positions and directions in the camera reference frame. The image processing part suggests a way how to apply for real applications. The error propagation analysis part discusses how much the estimation errors of the planar surface constants are affected by the noise contained in beam spot images. By experimental simulations we show how much estimation errors can be expected for a certain beam configuration. The operating characteristics of our algorithm is also discussed in the simulation part.

In this paper, we will use the camera reference frame to denote all 3-dimensional quantities. Our analysis will not depend on whether the coordinate system is right-handed or left-handed. By convention, the z-axis of the camera reference frame is the optical axis of the camera and its origin is at the *center of perspective projection*. All vectors and points will be represented by column vectors and a prime superscript will be used to denote the transposition of matrices.

2. Estimation

In this part we investigate the following : how well can we estimate the surface constants (surface normal and distance from the origin) of a planar work surface from the knowledge of the positions and orientations of laser beams together with the images of beam spots on the plane ?

2.1 Statement of the Problem

Let us assume that we know the positions and directions of laser beams. Consider the following set

$$P = \left\{ \begin{pmatrix} X_n \\ Y_n \\ Z_n \end{pmatrix} \;\middle|\; \begin{pmatrix} X_n \\ Y_n \\ Z_n \end{pmatrix} = \begin{pmatrix} x_n \\ y_n \\ z_n \end{pmatrix} + d_n \begin{pmatrix} a_n \\ b_n \\ c_n \end{pmatrix}, \right.$$
$$\left. a_n^2 + b_n^2 + c_n^2 = 1, \;\; n = 1, \cdots, N \right\} \quad (1)$$

where the $(x_n \;\; y_n \;\; z_n)'$ are the beam positions, the $(a_n \;\; b_n \;\; c_n)'$ are the beam directions and the d_n are scalars. If the point set P is on the planar surface $\Gamma : Ax + By + Cz + D = 0$ with $A^2 + B^2 + C^2 = 1$ and

$D < 0$, then we must have $AX_n + BY_n + CZ_n + D = 0$ for $n = 1, \cdots, N$.

Also we assume that we know the coordinates of image points of the beam spots on the planar work surface. The set of image points can be expressed as

$$\left\{ \begin{pmatrix} \hat{u}_n \\ \hat{v}_n \end{pmatrix} \Big| \begin{pmatrix} \hat{u}_n \\ \hat{v}_n \end{pmatrix} = \begin{pmatrix} u_n \\ v_n \end{pmatrix} + \begin{pmatrix} \Delta u_n \\ \Delta v_n \end{pmatrix}, n = 1, \cdots, N \right\} \tag{2}$$

The $(\hat{u}_n \ \hat{v}_n)'$ are the measured quatities, the $(u_n \ v_n)'$ are the perspective projections (of the laser beam spots on the planar surface) represented by

$$\begin{pmatrix} u_n \\ v_n \end{pmatrix} = \frac{f}{z_n + d_n c_n} \begin{pmatrix} x_n + d_n a_n \\ y_n + d_n b_n \end{pmatrix}, n = 1, \cdots, N \tag{3}$$

and the $(\Delta u_n \ \Delta v_n)'$ are the random errors(noise) contained in the measured quantities $(\hat{u}_n \ \hat{v}_n)'$. In (3), f denotes the focal length of the camera. In this paper, the random errors are assumed to be the identically independent Gaussian random vectors each of which has mean $\begin{pmatrix} 0 \\ 0 \end{pmatrix}$ and variance $\begin{pmatrix} \sigma^2 & 0 \\ 0 & \sigma^2 \end{pmatrix}$.

Now, we are given the positions and orientations of N beams as well as the measured image points $(\hat{u}_n \ \hat{v}_n)'$ of the beam spots on the plane Γ. We expect that the inverse projected points of the measured image points are the beam spots on the plane Γ. In practice, this rarely happens because the measured image points usually contain some amount of noise. For this reason, our goal should be the estimation of the plane equation $\Gamma : Ax + By + Cz + D = 0$ for which

$$\sum_{n=1}^{N} w_n[(\hat{u}_n - u_n)^2 + (\hat{v}_n - v_n)^2] \tag{4}$$

is minimized under the constraint that the beam spots $(X_n \ Y_n \ Z_n)'$ are on the same plane. If the beam spots $(X_n \ Y_n \ Z_n)'$ are to be on a plane represented by $Ax + By + Cz + D = 0$, we must have, for all n,

$$AX_n + BY_n + CZ_n + D = 0 \tag{5}$$

By averaging them out, we have

$$A\bar{X} + B\bar{Y} + C\bar{Z} + D = 0 \tag{6}$$

where $\bar{X} = (\sum_{n=1}^{N} X_n)/N$ and so on. From (5) and (6), we have, for all n,

$$A(X_n - \bar{X}) + B(Y_n - \bar{Y}) + C(Z_n - \bar{Z}) = 0 \tag{7}$$

which tells us that

$$\begin{pmatrix} X_n - \bar{X} \\ Y_n - \bar{Y} \\ Z_n - \bar{Z} \end{pmatrix} \perp \begin{pmatrix} A \\ B \\ C \end{pmatrix}, \quad n = 1, \cdots, N \tag{8}$$

This condition can be expressed in the following form :

$$\begin{aligned} & C(d_1, d_2, \cdots, d_N) \\ & = \det\left[\sum_{n=1}^{N} \begin{pmatrix} X_n - \bar{X} \\ Y_n - \bar{Y} \\ Z_n - \bar{Z} \end{pmatrix} \begin{pmatrix} X_n - \bar{X} \\ Y_n - \bar{Y} \\ Z_n - \bar{Z} \end{pmatrix}' \right] \\ & = 0 \end{aligned} \tag{9}$$

where det[.] denotes the determinant of its argument.

Use of a Lagrange multiplier will simplify our complicated constrained problem. Suppose that we have the function $E(d_1, d_2, \cdots, d_N)$ defined by

$$\begin{aligned} & E(d_1, d_2, \cdots, d_N) \\ & = \sum_{n=1}^{N} w_n[(\hat{u}_n - u_n)^2 + (\hat{v}_n - v_n)^2] \\ & \quad + \lambda C(d_1, d_2, \cdots, d_N) \end{aligned} \tag{10}$$

where λ is a Lagrange multiplier. The optimal condition on E will be

$$\frac{\partial E}{\partial d_n} = 0, \quad n = 1, \cdots, N \qquad \text{and} \qquad \frac{\partial E}{\partial \lambda} = 0 \tag{11}$$

Since it is impossible to find algebraic solutions to Eq. (11), we have to resort to numerical computation in order to minimize $E(d_1, d_2, \cdots, d_n)$. If we manage to find the global minimum point $(\hat{d}_1, \hat{d}_2, \cdots, \hat{d}_N)$ for $E(d_1, d_2, \cdots, d_n)$, the estimation of the surface constants A, B, C, and D can be done by taking any four equations from the overdetermined system (5). This numerical method requires some iterations.

In stead of numerical computation, what if we discard our constraint (9) and minimize each term of the first summation of (10)? This will greatly simplify our task and lead to algebraic solutions as can be seen in the subsequent sections. In this method, we first estimate each d_n in the least squares sense. And then, using these values of d_n, we estimate the surface constants of the planar surface under consideration as a solution of an eigenvalue problem.

Since the constraint (9) is not employed by the above algebraic method, it is not guaranteed that the so-obtained estimated beam spots lie entirely on a planar surface. So we might worry about whether the results of these two methods are very different. In fact, the two methods (*numerical and algebraic*) return different results every time. However, this fact is of little concern since we are in noisy environment. Either method will not give the exact surface parameters which can be a solution in noiseless case. Therefore, the important thing

is to compare the statistics returned by the two methods. Comparison of their statistics in Table 1 tells us that there is no big difference between the two methods.

2.2 Estimation of d_n

Under the assumption of Gaussian noise environment we can estimate the optimal value of d_n in the least squares sense. Let the objective function for each n be

$$\epsilon_n = (\hat{u}_n - u_n)^2 + (\hat{v}_n - v_n)^2 \tag{12}$$

Substituting (3) into (12) and expanding ϵ_n in partial fractions, this equation can be written as

$$\epsilon_n = \frac{R_n^2}{(z_n + d_n c_n)^2} + \frac{R_n^1}{(z_n + d_n c_n)} + R_n^0 \tag{13}$$

where

$$R_n^2 = f^2\{(z_n\frac{a_n}{c_n} - x_n)^2 + (z_n\frac{b_n}{c_n} - y_n)^2\} \tag{14.1}$$

$$R_n^1 = -2f\{(f\frac{a_n}{c_n} - \hat{u}_n)(z_n\frac{a_n}{c_n} - x_n) + (f\frac{b_n}{c_n} - \hat{v}_n)(z_n\frac{b_n}{c_n} - y_n)\} \tag{14.2}$$

$$R_n^0 = (f\frac{a_n}{c_n} - \hat{u}_n)^2 + (f\frac{b_n}{c_n} - \hat{v}_n)^2 \tag{14.3}$$

Note that Eq.(13) is a quadratic expression. We can easily see that ϵ_n becomes the minimum value when

$$z_n + d_n c_n = -\frac{2R_n^2}{R_n^1} \tag{15}$$

The optimal value $\hat{d_n}$ for each n is then calculated as

$$\hat{d_n} = -\frac{z_n}{c_n} - \frac{2R_n^2}{R_n^1 c_n} \tag{16}$$

These values will be used to estimate the surface constants in the subsequent subsection.

2.3 Estimation of the Surface Constants of the Plane Γ

With the optimal values of d_n, the estimated positions of the beam spots on the planar surface can be expressed as

$$\hat{P} = \left\{ \begin{pmatrix} p_n \\ q_n \\ r_n \end{pmatrix} \middle| \begin{pmatrix} p_n \\ q_n \\ r_n \end{pmatrix} = \begin{pmatrix} x_n \\ y_n \\ z_n \end{pmatrix} + \hat{d_n} \begin{pmatrix} a_n \\ b_n \\ c_n \end{pmatrix}, \quad a_n^2 + b_n^2 + c_n^2 = 1, \quad n = 1, \cdots, N \right\} \tag{17}$$

Now we estimate the equation of the planar surface $\Gamma : Ax + By + Cz + D = 0$ under the constraints that $A^2+B^2+C^2 = 1$ and $D < 0$. Since $\hat{P}$ is not guaranteed to lie entirely on Γ, the estimation will be done in the least squares sense. Using the Lagrange multiplier λ, the function to be minimized is

$$E_\lambda = \sum_{n=1}^{N} w_n(Ap_n+Bq_n+Cr_n+D)^2+\lambda(A^2+B^2+C^2-1) \tag{18}$$

The function E_λ has a minimum when

$$\frac{\partial E_\lambda}{\partial A} = \frac{\partial E_\lambda}{\partial B} = \frac{\partial E_\lambda}{\partial C} = \frac{\partial E_\lambda}{\partial D} = \frac{\partial E_\lambda}{\partial \lambda} = 0 \tag{19}$$

or

$$\overline{p^2}A + \overline{pq}B + \overline{pr}C + \bar{p}D + \lambda A = 0 \tag{20.1}$$

$$\overline{pq}A + \overline{q^2}B + \overline{qr}C + \bar{q}D + \lambda B = 0 \tag{20.2}$$

$$\overline{pr}A + \overline{qr}B + \overline{r^2}C + \bar{r}D + \lambda C = 0 \tag{20.3}$$

$$\bar{p}A + \bar{q}B + \bar{r}C + D = 0 \tag{20.4}$$

$$A^2 + B^2 + C^2 - 1 = 0 \tag{20.5}$$

where $\bar{p} = (\sum_{n=1}^{N} w_n p_n)/(\sum_{n=1}^{N} w_n)$ and so on. Substituting (20.4) into (20.1), (20.2) and (20.3), we get

$$\begin{aligned} (\overline{p^2} - \bar{p}^2)A + (\overline{pq} - \bar{p}\bar{q})B + (\overline{pr} - \bar{p}\bar{r})C + \lambda A = 0 \\ (\overline{pq} - \bar{p}\bar{q})A + (\overline{q^2} - \bar{q}^2)B + (\overline{qr} - \bar{q}\bar{r})C + \lambda B = 0 \\ (\overline{pr} - \bar{p}\bar{r})A + (\overline{qr} - \bar{q}\bar{r})B + (\overline{r^2} - \bar{r}^2)C + \lambda C = 0 \end{aligned} \tag{21}$$

or in matrix form

$$\begin{pmatrix} \overline{p^2} - \bar{p}^2 & \overline{pq} - \bar{p}\bar{q} & \overline{pr} - \bar{p}\bar{r} \\ \overline{pq} - \bar{p}\bar{q} & \overline{q^2} - \bar{q}^2 & \overline{qr} - \bar{q}\bar{r} \\ \overline{pr} - \bar{p}\bar{r} & \overline{qr} - \bar{q}\bar{r} & \overline{r^2} - \bar{r}^2 \end{pmatrix} \begin{pmatrix} A \\ B \\ C \end{pmatrix} + \lambda \begin{pmatrix} A \\ B \\ C \end{pmatrix} = 0 \tag{22}$$

From the above expression we notice that our minimization problem turns out to be an eigenvalue problem. It is well known that real symmetric matrices have real eigenvalues, the number of which is equal to the size of the matrix. To find the desired surface normal of the planar work surface, we have to choose the unit eigenvector $(A\ B\ C)'$ for which the function E

$$E = \sum_{n=1}^{N} w_n(Ap_n + Bq_n + Cr_n + D)^2 \tag{23}$$

takes on the minimum value. If we substitute (20.4) into (23), then we have

$$E = \sum_{n=1}^{N} w_n[(p_n - \bar{p})A + (q_n - \bar{q})B + (r_n - \bar{r})C]^2 \tag{24}$$

which can be written in a quadratic form

$$E = (A\ B\ C) \begin{pmatrix} \overline{p^2} - \bar{p}^2 & \overline{pq} - \bar{p}\bar{q} & \overline{pr} - \bar{p}\bar{r} \\ \overline{pq} - \bar{p}\bar{q} & \overline{q^2} - \bar{q}^2 & \overline{qr} - \bar{q}\bar{r} \\ \overline{pr} - \bar{p}\bar{r} & \overline{qr} - \bar{q}\bar{r} & \overline{r^2} - \bar{r}^2 \end{pmatrix} \begin{pmatrix} A \\ B \\ C \end{pmatrix} \tag{25}$$

Let the $\lambda_i (i = 1, 2, 3)$ be the eigenvalues of the 3×3 matrix appearing in (25) and the $(A_i \ B_i \ C_i)'$ be the corresponding unit eigenvectors. Then, for each λ_i, we have

$$E = (A_i B_i C_i)\lambda_i \begin{pmatrix} A_i \\ B_i \\ C_i \end{pmatrix} = \lambda_i \geq \lambda_{min} \qquad (26)$$

where λ_{min} is the smallest eigenvalue among $\{\lambda_1, \lambda_2, \lambda_3\}$. Now we can conclude that the estimated surface normal $(\hat{A} \ \hat{B} \ \hat{C})'$ is the unit eigenvector associated with the smallest eigenvalue of the symmetric matrix appearing in (25) and the estimate $\hat{D}$ is obtained by

$$\hat{D} = -\hat{A}\bar{p} - \hat{B}\bar{q} - \hat{C}\bar{r} \qquad (27)$$

If $\hat{D}$ is positive, then we should invert the direction of the unit eigenvector $(\hat{A} \ \hat{B} \ \hat{C})'$ by multiplying it by -1. This kind of eigenvalue problems can be easily solved with the existing software packages [1].

3. Calibration of Beam Positions and Orientations

In section 2, we estimated the surface constants of a planar work surface by assuming that we have a prior knowledge about the exact positions and orientations of laser beams projecting on the planar work surface. Prior to use, however, the setup must be carefully calibrated to determine precise values for the assumed quantities $(x_n \ y_n \ z_n)'$ and $(a_n \ b_n \ c_n)'$ for all n.

For calibration, we assume that the focal length f of the camera is known to us, that the principal point is at the center of the focal plane[3], that the optical axis is perpendicular to the image plane and that we can move each beam source mounted on a platform. These assumptions may be too strigent in some sense. However, the first three assumptions are related to the camera calibration, which is not a major concern in this paper.

3.1 Calibration of a Reference Point on the z-axis

Suppose that a plane is perpendicular to the optical axis. Then this plane will be represented by $z = h(> 0)$. Unfortunately, we do not know the exact value of h. Hence we need to estimate the value of h to a certain precision, which corresponds to the determination of the position of the optical center (center of perspectivity).

Let us consider the two points $\mathbf{x_1}$ and $\mathbf{x_2}$ on the plane $z = h$ which are represented by

$$\mathbf{x_1} = \begin{pmatrix} x_1 \\ y_1 \\ h \end{pmatrix}, \quad \mathbf{x_2} = \begin{pmatrix} x_2 \\ y_2 \\ h \end{pmatrix} \qquad (28)$$

and the corresponding image points which are represented by

$$\mathbf{u_1} = \begin{pmatrix} u_1 \\ v_1 \end{pmatrix} = \frac{f}{h}\begin{pmatrix} x_1 \\ y_1 \end{pmatrix} \qquad (29.1)$$

$$\mathbf{u_2} = \begin{pmatrix} u_2 \\ v_2 \end{pmatrix} = \frac{f}{h}\begin{pmatrix} x_2 \\ y_2 \end{pmatrix} \qquad (29.2)$$

Then the distance between $\mathbf{u_1}$ and $\mathbf{u_2}$ is

$$\rho_{12} = \sqrt{(u_1 - u_2)^2 + (v_1 - v_2)^2} \qquad (30)$$

and the distance between $\mathbf{x_1}$ and $\mathbf{x_2}$ is

$$r_{12} = \sqrt{(x_1 - x_2)^2 + (y_1 - y_2)^2} \qquad (31)$$

From (29), (30) and (31), we have

$$\rho_{12} = \frac{f}{h} r_{12} \qquad (32)$$

or

$$h = f\frac{r_{12}}{\rho_{12}} \qquad (33)$$

which tells us that if we know the distance between two points on the plane $z = h$ and the corresponding distance in the image plane, we can determine the value of d. Here, a comment may be made on the relationship: We have to take into consideration a certain amount of measurement error in the distance r_{12} on $z = h$ and a certain amount of measurement error in the distance ρ_{12} on the image plane. If the measurement errors of interest are assumed to be small, then we have, from (33),

$$\frac{\Delta h}{h} = \frac{\Delta r_{12}}{r_{12}} - \frac{\Delta \rho_{12}}{\rho_{12}} \qquad (34)$$

As r_{12} and ρ_{12} become larger, the positional error Δh becomes smaller.

3.2 Calibration of Beam Positions and Orientations

Let us consider the points $P_1, \cdots, P_N$ on the plane $z = d_1$

$$P_1 = \begin{pmatrix} x_1 \\ y_1 \\ d_1 \end{pmatrix}, \cdots, P_N = \begin{pmatrix} x_N \\ y_N \\ d_1 \end{pmatrix} \qquad (35)$$

and the points $Q_1, \cdots, Q_N$ on the plane $z = d_2$

$$Q_1 = \begin{pmatrix} x_1 \\ y_1 \\ d_2 \end{pmatrix}, \cdots, Q_N = \begin{pmatrix} x_N \\ y_N \\ d_2 \end{pmatrix} \qquad (36)$$

where $d_1 > d_2$. Then we can adjust the beam positions and orientations so that the x and y components of the n-th beam position $(x_n\ y_n\ z_n)'$, $n = 1, \cdots, N$ are equal to those of P_n (or Q_n), respectively, and the n-th beam passes through both P_n and Q_n. If $d_1 - d_2$ is large enough, then these beams are, in effect, parallel to the optical axis.

Now we have to determine the z component of each beam position to a certain precision. We can change the orientations of the laser beams to focus at a certain point on the plane $z = d_2$. Let the point be $(0\ 0\ d_1)'$. Then the point on the plane $z = d_1$ through which the laser beam emanating from $(x_n\ y_n\ z_n)'$ passes will be $(x_{n0}\ y_{n0}\ d_2)'$ where

$$x_{n0} = \frac{d_1 - d_2}{d_1 - z_n} x_n, \quad y_{n0} = \frac{d_1 - d_2}{d_1 - z_n} y_n \tag{37}$$

and its perspective projection will be

$$\begin{pmatrix} u_{n0} \\ v_{n0} \end{pmatrix} = \frac{f}{d_2} \begin{pmatrix} x_{n0} \\ y_{n0} \end{pmatrix} = \frac{f}{d_2} \left(\frac{d_1 - d_2}{d_1 - z_n} \right) \begin{pmatrix} x_n \\ y_n \end{pmatrix} \tag{38}$$

from which we have

$$\sqrt{u_{n0}^2 + v_{n0}^2} = \frac{f}{d_2} \left(\frac{d_1 - d_2}{d_1 - z_n} \right) \sqrt{x_n^2 + y_n^2} \tag{39}$$

or

$$z_n = d_1 - (d_1 - d_2) \frac{f}{d_2} \frac{\sqrt{x_n^2 + y_n^2}}{\sqrt{u_{n0}^2 + v_{n0}^2}} \tag{40}$$

We follow the above procedure repeatedly to calibrate the positions of all laser beams.

If our calibration point is located at $(0\ 0\ d_1)'$, then the orientation of each beam can be obtained by normalizing the vector from the beam source position to the calibration point. We don't need, however, the procedure from (37) through (40) if we desire a parallel beam pattern. In that case, it suffices that z components of all source positions are set to be zero.

4. Image Processing

In previous sections we have implicitly assumed that we can determine the coordinates of beam spots on the image plane. We need to contemplate on it since each beam spot image occupies some area (usually, over 100 pixels) on the image plane.

A CCD camera contains an array of photodetectors, a set of electronic switches, and control circuitry on a single chip. By external clocking, the array can be scanned element by element in any desired manner and a video signal is output. This video signal is analog in nature. To process the image by use of a computer, it is necessary to convert the incoming signal to a digital form, which can be accomplished through the use of A/D converters. Digital images produced as such are usually stored in a frame grabber for processing. If the horizontal spacing between consecutive photodetectors is not the same as the vertical spacing on a CCD array, the aspect-ratio-correction may be required to obtain a digitized image in square pixel format, where the actual spatial dimensions of each pixel will be 1 unit in the horizontal direction and 1 unit in the vertical.

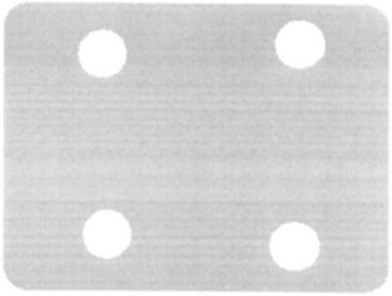

Fig 3. An Image displayed on the TV monitor

Images obtained with the SHEE consist of a background and several disk-like regions (Fig 3). Each disk-like region corresponds to a laser beam. Our analysis in previous sections completely depends on the determination of image coordinates.

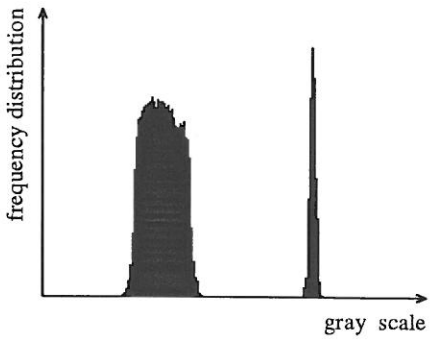

Fig 4. Histogram for the Image shown in Fig 3

If background lighting is arranged so as to be fairly uniform, and we are looking for such regions that can be contrasted against a background, segmentation can be achieved simply by thresholding the image at a particular intensity level. Ambient light illumination and collimated beam spots are the two factors which contribute to the histogram of our images. If the

intensity of ambient light illumination is a rather uniform, the distribution of gray scale values of beam spot images can be made well separated from the distribution of those of a background by adjusting the intensity of beam sources (Fig 4). The peak on the left of the histogram corresponds to ambient light and the peak on the right corresponds to collimated beams. If there is no overlapping region for the two distribution, then any values in the separating region can be chosen as a thresholding level for segmentation. By taking a centroid of each segmented region, we obtain the coordinates of beam spot images. During this process, local interactions between adjacent CCD array elements may blur the image to be processed if the intensity of beam sources is high. When blurring occurs, the use of polarizers is recommended to reduce such a degradation phenomenon.

Though the coordinates of beam spot images can be obtained in the above way, there still exists a problem. That is, they are represented in pixel units. Unless the physical dimension of the CCD array and A/D conversion mechanism are known, some conversion scheme has to be provided experimentally so that the coordinates of image points be represented in usual distance units such as millimeters or inches. Let us consider the nonoverlapping two circular regions C_1 and C_2 marked on the plane Γ at $z = h$. Let d denote the measured center-to-center distance between C_1 and C_2. We take the image and process it according to the above method. Finally we can get the center-to-center distance in pixel units. Let the distance be denoted by n_h. Now, we move the plane Γ to $z = h + \Delta h$. In a similar way, we can get another center-to-center distance $n_{h+\Delta h}$ in pixel units. Let the pixel spacing be δ, which corresponds to the actual distance between consecutive pixels within the camera coordinate system. Then the actual distances for n_h and $n_{h+\Delta h}$ will be represented by $n_h\delta$ and $n_{h+\Delta h}\delta$. Using eq (32), we have the following relationship :

$$n_h\delta h = n_{h+\Delta h}\delta(h + \Delta h)$$

from which we have

$$h = \frac{n_{h+\Delta h}}{(n_h - n_{h+\Delta h})}\Delta h$$

Finally we have

$$\delta = \frac{(n_h - n_{h+\Delta h})}{n_h n_{h+\Delta h}} f d \Delta h$$

This conversion factor enables us to get coordinates of image points in usual distance units. Of course, it is important to measure the quantities d and Δh as precisely as possible.

5. Error Propagation

In this part we see how the estimated surface constants $\hat{A}$, $\hat{B}$, $\hat{C}$ and $\hat{D}$ are affected by noise contained in the image points. For this purpose we will find the covariance matrix for the surface constants. We know that the planar work surface can be estimated from a knowledge of beam positions $\mathbf{x_n} = (x_n \ y_n \ z_n)'$ and orientations $\mathbf{a_n} = (a_n \ b_n \ c_n)'$ and the corresponding image points $\hat{\mathbf{u}}_\mathbf{n} = (\hat{u}_n \ \hat{v}_n)'$, $n = 1, \cdots, N$. As mentioned earlier, the image points can be written as

$$\hat{\mathbf{u}}_\mathbf{n} = \mathbf{u_n} + \mathbf{\Delta u_n}, \qquad n = 1, \cdots, N \tag{41}$$

where $\mathbf{u_n} = (u_n \ v_n)'$ and $\mathbf{\Delta u_n} = (\Delta u_n \ \Delta v_n)'$. The information we have about $\mathbf{\Delta u_1}, \cdots, \mathbf{\Delta u_N}$ is that they are the identically independent Gaussian random vectors with

$$\begin{aligned} E[\mathbf{\Delta u_n}] &= \begin{pmatrix} 0 \\ 0 \end{pmatrix} \\ E[\mathbf{\Delta u_n \Delta u_n}'] &= \begin{pmatrix} \sigma^2 & 0 \\ 0 & \sigma^2 \end{pmatrix}, \quad n = 1, \cdots, N \\ E[\mathbf{\Delta u_n \Delta u_m}'] &= \begin{pmatrix} 0 & 0 \\ 0 & 0 \end{pmatrix} \quad , \ n \neq m \end{aligned} \tag{42}$$

Note that the surface constants A, B, C, D depend on the $\mathbf{u_n}$ through our noiseless model, for each n,

$$\begin{aligned} &f(\mathbf{x_n}, \mathbf{a_n}, d_n(\mathbf{u_n}), \beta) \\ &\quad = A(x_n + d_n(\mathbf{u_n})a_n) + B(y_n + d_n(\mathbf{u_n})b_n) \\ &\quad\quad + C(z_n + d_n(\mathbf{u_n})c_n) + D = 0 \end{aligned} \tag{43}$$

where $\beta = (A \ B \ C \ D)'$. If the quantities $\mathbf{u_n} + \mathbf{\Delta u_n}$ are observed, then the quantities $A + \Delta A$, $B + \Delta B$, $C + \Delta C$, $D + \Delta D$ are determined to satisfy the idealized model, for each n,

$$f(\mathbf{x_n}, \mathbf{a_n}, d_n(\mathbf{u_n} + \mathbf{\Delta u_n}), \beta + \Delta\beta) = 0 \tag{44}$$

where $\Delta\beta$ represents $(\Delta A \, \Delta B \, \Delta C \, \Delta D)'$. The errors $\mathbf{\Delta u_1}, \cdots, \mathbf{\Delta u_N}$ induce an error $\Delta\beta$ in the calculated $\beta + \Delta\beta$. The error propagation analysis determines what the expected value of $\beta + \Delta\beta$ is and what the variance of $\beta + \Delta\beta$ is. If the random errors $\mathbf{\Delta u_1}, \cdots, \mathbf{\Delta u_N}$ are small, we can approximate our noisy model (44) as

$$\begin{aligned} &f(\mathbf{x_n}, \mathbf{a_n}, d_n(\mathbf{u_n} + \mathbf{\Delta u_n}), \beta + \Delta\beta) \\ &\quad = f(\mathbf{x_n}, \mathbf{a_n}, d_n(\mathbf{u_n}), \beta) + g_n'\mathbf{\Delta u_n} + h_n'\Delta\beta \end{aligned} \tag{45}$$

where the g_n and h_n are the gradients of f with respect to $\mathbf{u_n}$ and β evaluated at $(\mathbf{u_n}, \beta)$, that is,

$$g_n = \left(\frac{\partial f}{\partial u_n} \quad \frac{\partial f}{\partial v_n} \right)' \tag{46.1}$$

and

$$h_n = \left(\frac{\partial f}{\partial A} \quad \frac{\partial f}{\partial B} \quad \frac{\partial f}{\partial C} \quad \frac{\partial f}{\partial D} \right)' \tag{46.2}$$

With the above two models, we have

$$\begin{pmatrix} g_1' \Delta \mathbf{u_1} \\ \vdots \\ g_N' \Delta \mathbf{u_N} \end{pmatrix} + H \begin{pmatrix} \Delta A \\ \Delta B \\ \Delta C \\ \Delta D \end{pmatrix} = 0 \tag{47}$$

where H is defined by

$$H = \begin{pmatrix} h_1' \\ \vdots \\ h_N' \end{pmatrix} \tag{48}$$

Let the sigular value decomposition[1] of H be

$$H = USV' \tag{49}$$

Then the least squares solution of the overdetermined system (47) is given by

$$\Delta\beta = -VS^{-1}U' \begin{pmatrix} g_1' \Delta \mathbf{u_1} \\ \vdots \\ g_N' \Delta \mathbf{u_N} \end{pmatrix} \tag{50}$$

From this expression it is clear that to the extent the linearization approximation (47) is good, the expected value of $\Delta\beta$ is 0 under our noise model (42), that is,

$$E[\Delta\beta] = 0 \tag{51}$$

To determine the covariance matrix of $\beta + \Delta\beta$ we examine

$$\begin{aligned} \Delta\beta\Delta\beta' =& VS^{-1}U' \begin{pmatrix} g_1' \Delta \mathbf{u_1} \\ \vdots \\ g_N' \Delta \mathbf{u_N} \end{pmatrix} \\ & (\Delta \mathbf{u_1}' g_1 \cdots \Delta \mathbf{u_N}' g_N)\, US^{-1}V' \end{aligned} \tag{52}$$

With the assumption (42) the expectation of $\Delta\beta\Delta\beta'$ gives the following covariance matrix :

$$\begin{aligned} E(\Delta\beta\Delta\beta') &= VS^{-1}U' \begin{pmatrix} g_1' E(\Delta \mathbf{u_1} \Delta \mathbf{u_1}') g_1 & & \\ & \ddots & \\ & & g_N' E(\Delta \mathbf{u_N} \Delta \mathbf{u_N}') g_N \end{pmatrix} US^{-1}V' \\ &= \sigma^2 VS^{-1}U'DUS^{-1}V' \end{aligned} \tag{53}$$

where

$$D = \begin{pmatrix} g_1' g_1 & & \\ & \ddots & \\ & & g_N' g_N \end{pmatrix} \tag{54}$$

Notice that this analytical form is dependent on σ^2, the $\{\mathbf{x_n}, \mathbf{a_n}\}_{n=1,\cdots,N}$ and β. This covariance matrix provides us with a measure of uncertainty in the estimated surface constants.

6. Experiment

6.1 Error Measures

Our experiments are concerned with how much the estimated surface constants $\hat{A}$, $\hat{B}$, $\hat{C}$ and $\hat{D}$ will deviate from the true values A, B, C and D. The first three parameters A, B, C represent the direction of the surface normal. Since the angle γ between the true surface normal and the estimated one

$$\gamma = cos^{-1}(A\hat{A} + B\hat{B} + C\hat{C}) \tag{55}$$

will describe this discrepancy, we use this angle as an error measure of direction. The last parameter D represents the distance from the origin to the planar work surface. We need to describe a difference between the true value D and its estimate $\hat{D}$. Another error measure for this purpose is defined as

$$\delta = \left| \hat{D} - D \right| \tag{56}$$

Note that the distribution of error measures of direction is a circular distribution. The mean direction $\bar{\gamma}$ of $\gamma_1, \cdots, \gamma_n$ is defined to be the direction of the *resultant* (vector sum) of the unit vectors $(cos\gamma_1\ sin\gamma_1)', \cdots, (cos\gamma_n\ sin\gamma_n)'$. And a meaningful measure of dispersion for a circular distribution is the circular variance S_γ defined to be

$$S_\gamma = 1 - \bar{R} \tag{57}$$

where $\bar{R}$ is the mean resultant length [2]

$$\bar{R} = \sqrt{(\frac{1}{n}\sum_{i=1}^{n} cos\gamma_i)^2 + (\frac{1}{n}\sum_{i=1}^{n} sin\gamma_i)^2} \tag{58}$$

The mean and variance of the distance errors will be obtained in a usual way. The mean distance error $\bar{\delta}$ of $\delta_1, \cdots, \delta_n$ is defined as

$$\bar{\delta} = \frac{1}{n}\sum_{i=1}^{n} \delta_i \tag{59}$$

and their variance $Var(\delta)$ is defined as

$$Var(\delta) = \frac{1}{n}\sum_{i=1}^{n}(\delta_i - \bar{\delta})^2 \qquad (60)$$

6.2 Error Rate

In the next subsection, we will see that there are four parameters to be controlled in the experiments, namely, a, p, σ and d. Our experiments will be done by varying two of them with others fixed. The results will be given in the form of graphs to show the error variations versus σ for each parameter setting. And we will discuss the influence of them on the performance of our algorithm.

The output of our algorithm will be analyzed in the following way: If the positions and orientations of the laser beams are carefully calibrated, then the errors contained in the image points will produce small errors in the surface constants. Since in practice we do not know the true values of the surface constants, we will use the covariance matrix to determine whether we accept an estimate (output of the software) or not. We define

$$V_{ABC} = Var(A) + Var(B) + Var(C) \qquad (61)$$

where $Var(A)$, $Var(B)$, and $Var(C)$ are estimated variances of surface normals A, B, and C, respectively. If $V_{ABC} \leq V_0$, then the estimates are declared to be accepted. Unfortunately, it is the case that the decisions made in this way are sometimes in error. There are two kinds of errors, false alarm rate and misdetection rate [4]. A false alarm rate P_F is the probability that an estimate cannot be accepted in the above sense though in fact the error is small. And a misdetection rate P_M is the probability that an estimate is accepted when in fact the error is large. That is,

$$P_F = Pr(V_{ABC} > V_0 \mid \gamma \leq \gamma_0) \qquad (62.1)$$

$$P_M = Pr(V_{ABC} \leq V_0 \mid \gamma > \gamma_0) \qquad (62.2)$$

These errors can be calculated by using the following numbers :

1. TT : the number of trials in which $V_{ABC} \leq V_0$ and $\gamma \leq \gamma_0$.
2. TF : the number of trials in which $V_{ABC} \leq V_0$ and $\gamma > \gamma_0$.
3. FT : the number of trials in which $V_{ABC} > V_0$ and $\gamma \leq \gamma_0$.
4. FF : the number of trials in which $V_{ABC} > V_0$ and $\gamma > \gamma_0$.

The sum of the above four numbers is equal to the number of experiments. From (62), the false alarm rate P_F is

$$P_F = \frac{FT}{FT + TT} \qquad (63)$$

and the misdetection rate P_M is

$$P_M = \frac{TF}{TF + FF} \qquad (64)$$

These error rates will characterize our algorithm. Through experiments, we will calculate these errors to obtain the operating characteristics of our algorithm.

6.3 Experiments

6.3.1 Experimental Protocol

Our problem is tested by generating simulated data with various amounts of noise and measuring the performance as a function of the amount of noise and the values of the experimental parameters. Since a camera equipped with a CCD array is promising for real-time processing applications, we will perform the experiments which can simulate such applications. Now we select one among the commercially available CCD cameras. The following is the specifications of the selected camera :

1. focal length f = 17.5 mm
2. equipped with a 1/2 inch CCD (570H×485V picture elements)
3. scan area of 6.39 × 4.88 mm
4. shooting distance of 20 mm thru ∞
5. framing angle of approx. 35° × 45° (at ∞)

As discussed earlier, our problem is to estimate the equation of a planar surface given a certain number of beam projectors with known positions and directions as well as the noisy image points corresponding to the beam spots on the planar surface. For our experiments, it is assumed that these beam sources are movable on a platform. Also it is assumed that the number of beam projectors is four since that number is limited in real applications. Notice that the beam projectors, in practice, emit beams each of which transversal cross section has a certain area. Then each of our image points will occupy a certain area on the image plane. The area is a collection of pixels whose gray scale values are higher than those of the background. To get the coordinates

of the image points, we may use the thresholding and centroiding techniques. Those values always contain some amounts of uncertainties. For our experiments such uncertainties are assumed to be Gaussian noise with mean 0 and standard deviation σ. Taking the above discussions into consideration, we perform our experiments which consist of the following steps (*all distances units are represented in millimeters*) :

1. The four beams are located at $(a, a, 0)$, $(-a, a, 0)$, $(-a, -a, 0)$ and $(a, -a, 0)$ and are made to be focused at $(0, 0, p)$ which we call the calibration point.
2. Choose a plane (work surface) defined by $x \cos\theta \cos\phi + y \cos\theta \sin\phi + z \sin\theta - d = 0$.
3. Determine the beam spot on the planar work surface corresponding to each beam source.
4. Find perspective projections of the 3-D beam spots and add identically independent Gaussian noise with mean 0 and standard deviation σ to each component to get the image point set.
5. For each image point, find the distance between the beam source and the 3-D beam spot in the least squares sense. Then we get the estimated locations of the beam spots.
6. From the estimated locations of 3-D beam spots, we estimate the surface constants of the planar work surface in the least squares sense.
7. Calculate the errors between the true values and the estimated ones of the surface constants using the error measures described in Section 5.1.

As can be seen in the above steps, the experimental parameters that can be controlled are a, p, θ, ϕ, d and σ. Several experiments will be done by varying these parameters. Estimation of surface constants will be done with the eigensystem method discussed in Section 2.2 and 2.3. We will use the error measures in Section 6.1 and the error rates in Section 6.2 to characterize the performance of our algorithm. In the first four expeiments, θ and ϕ will be varied uniformly in $[0°, 30°]$ and $[0°, 360°]$, respectively.

6.3.2 Experiment 1

We would like to find how the surface constants are affected by the calibration point and the noise standard deviation. For this purpose, set $a = 35$ and $d = 200$ and vary p from 350 to 500 in steps of 50 and σ from 0.005 to 0.02 in steps of 0.005. For each parameter setting, repeat steps from 1 to 7 at least one thousand times and calculate the mean and variance of error measures defined in section 6.1. In this experiment, we will also use parallel beams. Fig 5 tells us that errors become smaller as the calibration point approaches to infinity.

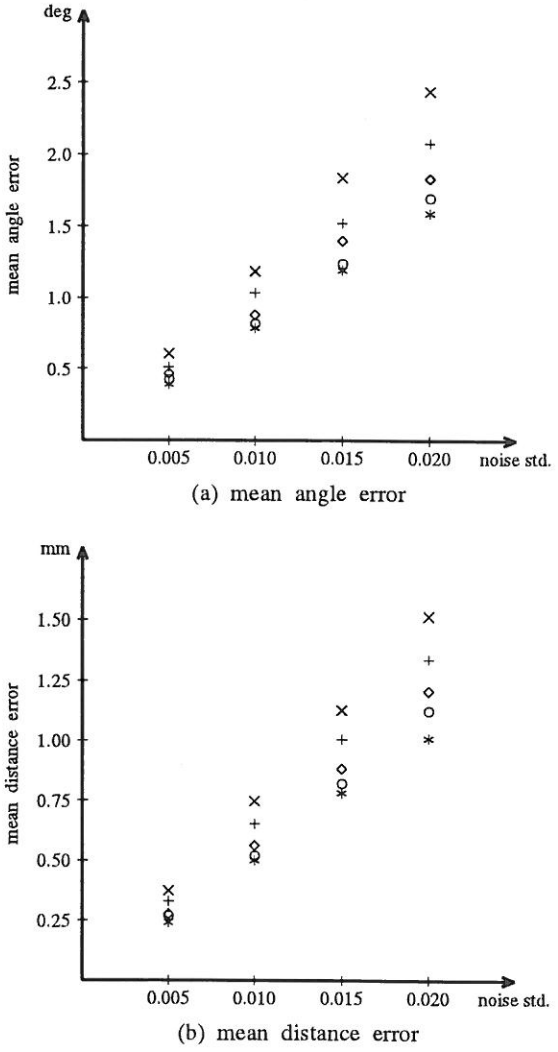

Fig 5. Performance characteristics for various calibration parameter values when the beam location and distance parameters are set to $a = 35$ and $d = 200$ while θ and ϕ are varied in $[0°, 30°]$ and $[0°, 360°]$, respectively :$\times$ when $p = 350$, $+$ when $p = 400$, $\diamond$ when $p = 450$, $\circ$ when $p = 500$, and $*$ when $p = \infty$.

6.3.3 Experiment 2

We would like to find how the surface constants are affected by the size parameter of the laser beams and the the noise standard deviation. For this purpose, set $p = 500$ and $d = 200$ and vary a from 25 to 40 in steps of 5 and σ from 0.005 to 0.02 in steps of 0.005. For each parameter setting, repeat steps from 1 to 7 at least one thousand times and calculate the mean and variance of error measures defined in section 6.1. Fig 6 tells us that errors become smaller as the beam location size parameter becomes larger.

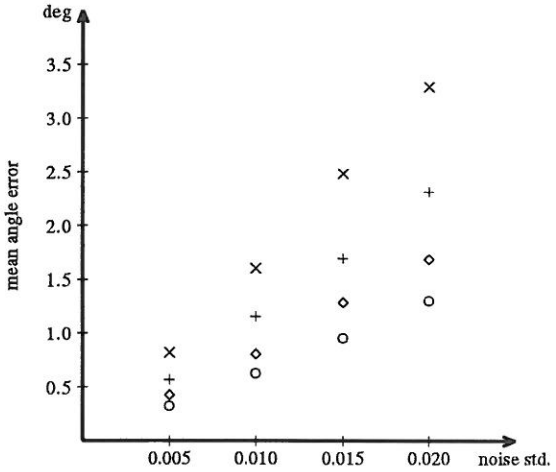

(a) mean angle error

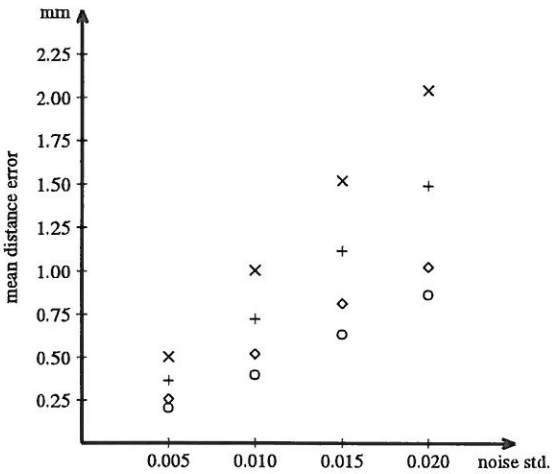

(b) mean distance error

Fig 6. Performance characteristics for various beam location parameter values when the calibration and distance parameters are set to $p = 500$ and $d = 200$ while θ and ϕ are varied in $[0°, 30°]$ and $[0°, 360°]$, respectively : $\times$ when $a = 25$, $+$ when $a = 30$, $\diamond$ when $a = 35$, and $\circ$ when $a = 40$.

6.3.4 Experiment 3

We would like to find how the surface constants are affected by the position of the work surface and the noise standard deviation. For this purpose, set $a = 35$ and $p = 500$ and vary d from 200 to 260 in steps of 20 and σ from 0.005 to 0.02 in steps of 0.005. For each parameter setting, repeat steps from 1 to 7 at least one thousand times and calculate the mean and variance of error measures defined in section 6.1. Fig 7 tells us that errors become smaller as the distance to the work surface becomes smaller.

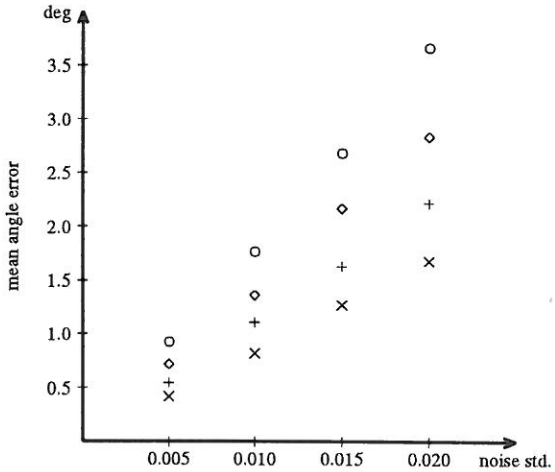

(a) mean angle error

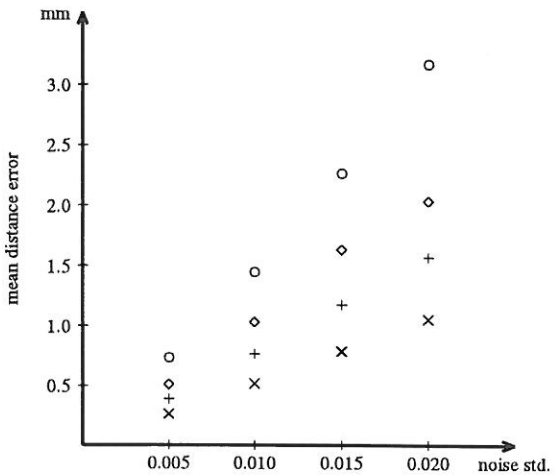

(b) mean distance error

Fig 7. Performance characteristics for various distance parameter values when the beam location and calibration parameters are set to $a = 35$ and $p = 500$ while θ and ϕ are varied in $[0°, 30°]$ and $[0°, 360°]$, respectively : $\times$ when $d = 200$, $+$ when $a = 220$, $\diamond$ when $a = 240$, and $\circ$ when $a = 260$.

6.3.5 Experiment 4

The covariance matrix is given by (53). Since this analytical form does not directly tell us of the operating characteristics of our software, we will resort to experiments. In this experiment, we set $a = 25$, $p = 500$, $d = 200$ and $\sigma = 0.005$. For this parameter setting, repeat steps from 1 to 6 at least one thousand times, each of which we calculate angle error between the true and the estimate surface normal and find the corresponding covariance matrix. For these values, calculate the false alarm rate and misdetection rate, varing V_0 within $[0.00090, 0.00135]$ in steps of 0.00005 and γ_0 within $[1°, 5°]$ in steps of $2°$. The results are shown in Fig 8.

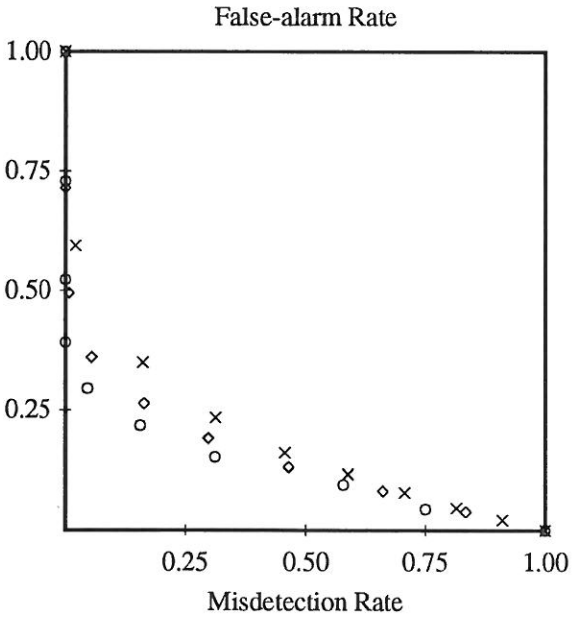

Fig 8. Operating Characteristic Curves for $a = 25$, $p = 500$, $d = 200$ and $\sigma = 0.005$ while θ and ϕ are chosen randomly in $[0°, 30°]$ and $[0°, 360°]$, respectively : $\times$ when $\gamma_0 = 1°$, $\diamond$ when $\gamma_0 = 3°$, $\circ$ when $\gamma_0 = 5°$.

6.3.6 Experiment 5

We used the covariance formula (44) in Experiment 4. Here we would like to verify its consistency experimentally. For this purpose, set $a = 35$, $p = 500$, $d = 200$, $\theta = 15°$, $\phi = 60°$ and vary σ from 0.005 to 0.02 in steps of 0.005. For each parameter setting, repeat steps from 1 to 7 at least one thousand times and calculate the mean and variance of error measures defined in section 6.1. Table 2 tells us that the experimental results comply with our error propagation analysis.

6.3.7 Experiment 6

In the first three experiments, we have selected θ randomly in $[0°, 30°]$. However, the performances are expected to vary for various θ's. In this experiment, we are interested in the sensitivity of error measures due to the variation of θ in that region. For this purpose, we set $a = 35$, $p = 500$, $d = 200$ and $\sigma = 0.005$ and repeat steps from 1 to 6 at least one thousand times. It turns out that performances are effectively the same along the azimuthal direction. Fig 9 shows the performance characteristics of our algorithm for various values of θ. Notice that estimation errors are the smallest when the plane is perpendicular to the optical axis.

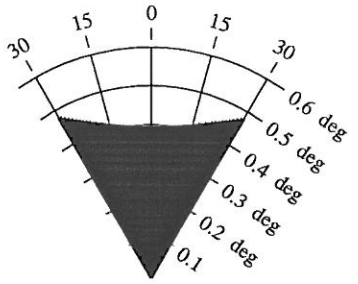

(a) mean angle error

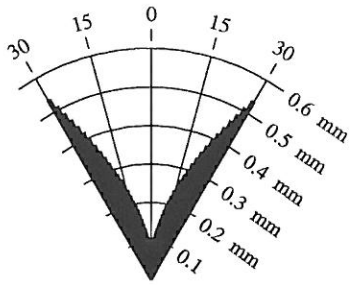

(b) mean distance error

Fig 9. Directional performance characteristics for $a = 35$, $p = 500$, $d = 200$ and $\sigma = 0.005$ while θ is varied from $0°$ to $30°$ in steps of $1°$.

7. Discussion

Our experiments were done on the assumption that only Gaussian noise is involved. Although the noise distribution to be considered in our problem may not be Gaussian, our analysis and experiments under the assumption give us valuable information on what we should do in order to make estimation errors small. The experimental results tell us that the larger the image size (consisting of four image points) is, the smaller the estimation error is. The diverging beam pattern may give better results than the converging one since the image size is less sensitive to the variation of distances from the optical center to the planar surface under consideration.

A particular beam pattern was employed for our experimental purpose. The desired beam pattern should be the one for which the amount of uncertainty in the estimated surface constants is minimized. Unfortunately, it is not easy to find it since the covariance matrix (53) is not a separable form for the parameters involved. There is one more thing we have to take into consideration. When images are taken by a camera with CCD array whose size is limited, all image points are not expected to lie on the scanning area of the CCD array for an arbitrary beam pattern. Note that the desired beam pattern is constrained by the following factors :

1. framing angle of a camera
2. range of the polar angle of the surface normal of the planar work surface
3. range of the distance from the camera to the planar work surface

Keeping these in mind, try to find the best beam pattern for your purpose.

REFERENCES

[1] William H. Press et al, *Numerical Recipes in C*, Cambridge University Press, 1988.

[2] K. V. Mardia, *Statistics of Directional Data*, Academic Press, 1972.

[3] Paul R. Wolf, *Elements of Photogrammetry*, McGraw Hill Inc., 1983.

[4] Robert M. Haralick, "Performance Assessment of Near Perfect Machines," Machine Vision and Applications 2:1-16, 1989.

Table 1. Statistics of numerical and algebraic solutions (the experimental protocol in section 6.3.1 applies to this experiment) : (a) $a = 35$, $p = \infty$, $d = 200$, and $\sigma = 0.005$ (b) $a = 35$, $p = \infty$, $d = 200$, and $\sigma = 0.010$

		numerical solution				algebraic solution			
(a)	1st moment	0.000283	0.000119	- 0.000094	0.017683	0.000292	0.000127	- 0.000097	0.018265
	2nd moment	0.005194	0.005155	0.001370	0.286281	0.005197	0.005170	0.001377	0.288548
	3rd moment	- 0.094386	- 0.021583	- 0.032779	- 0.022318	- 0.080924	- 0.023387	- 0.028049	- 0.018708
	4th moment	0.053572	0.030234	0.183477	0.143661	0.089820	0.031032	0.175099	0.131214
	covariance matrix	0.000027	- 0.000001	- 0.000003	0.000638	0.000027	- 0.000000	- 0.000004	0.000652
		- 0.000001	0.000027	- 0.000006	0.001178	- 0.000000	0.000027	- 0.000006	0.001193
		- 0.000003	- 0.000006	0.000002	- 0.000359	- 0.000004	- 0.000006	0.000002	- 0.000364
		0.000638	0.001178	- 0.000359	0.081957	0.000652	0.001193	- 0.000364	0.083260
(b)	1st moment	0.000265	- 0.000578	- 0.000026	0.004539	0.000213	- 0.000591	- 0.000016	0.002427
	2nd moment	0.010762	0.010793	0.002780	0.592500	0.010778	0.010826	0.002794	0.595689
	3rd moment	- 0.019399	- 0.174728	0.037547	- 0.027667	- 0.022936	- 0.179117	0.026182	- 0.017685
	4th moment	- 0.093388	- 0.029517	0.039069	0.032538	- 0.080536	- 0.006018	0.044454	0.079689
	covariance matrix	0.000116	- 0.000009	- 0.000013	0.002662	0.000116	- 0.000008	- 0.000014	0.002700
		- 0.000009	0.000116	- 0.000026	0.005008	- 0.000008	0.000117	- 0.000026	0.005059
		- 0.000013	- 0.000026	0.000008	- 0.001513	- 0.000014	- 0.000026	0.000008	- 0.001530
		0.002662	0.005008	- 0.001513	0.351056	0.002700	0.005059	- 0.001530	0.354846

Table 2. Experiments for verifying the error propagation analysis in section 5 (the experimental protocol in section 6.3.1 applies to this experiment) : The experimental parameters are set to $a = 35$, $p = 500$, $d = 200$, $\theta = 15°$, $\phi = 60°$, and (a) $\sigma = 0.005$, (b) $\sigma = 0.010$, (c) $\sigma = 0.015$, (d) $\sigma = 0.020$.

		analysis				experimental results			
(a)	mean	0.000000	0.000000	0.000000	0.000000	0.000313	0.000135	- 0.000107	0.020203
	covariance matrix	0.000033	- 0.000002	- 0.000004	0.000773	0.000031	- 0.000001	- 0.000004	0.000760
		- 0.000002	0.000031	- 0.000007	0.001338	- 0.000001	0.000031	- 0.000007	0.001386
		- 0.000004	- 0.000007	0.000002	- 0.000414	- 0.000004	- 0.000006	0.000002	- 0.000424
		0.000773	0.001338	- 0.000414	0.094309	0.000760	0.001386	- 0.000424	0.095150
(b)	mean	0.000000	0.000000	0.000000	0.000000	0.000230	- 0.000637	- 0.000028	0.004657
	covariance matrix	0.000132	- 0.000007	- 0.000016	0.003090	0.000134	- 0.000010	- 0.000016	0.003131
		- 0.000007	0.000123	- 0.000028	0.005351	- 0.000010	0.000136	- 0.000030	0.005875
		- 0.000016	- 0.000028	0.000009	- 0.001656	- 0.000016	- 0.000030	0.000009	- 0.001776
		0.003090	0.005351	- 0.001656	0.377237	0.003131	0.005875	- 0.001776	0.404675
(c)	mean	0.000000	0.000000	0.000000	0.000000	0.000536	- 0.000196	- 0.000353	0.072045
	covariance matrix	0.000296	- 0.000016	- 0.000036	0.006953	0.000327	- 0.000027	- 0.000037	0.007428
		- 0.000016	0.000227	- 0.000062	0.012040	- 0.000027	0.000284	- 0.000062	0.012144
		- 0.000036	- 0.000062	0.000019	- 0.003725	- 0.000037	- 0.000062	0.000019	- 0.003822
		0.006953	0.012040	- 0.003725	0.848783	0.007428	0.012144	- 0.003822	0.870428
(d)	mean	0.000000	0.000000	0.000000	0.000000	0.000244	0.000248	- 0.000650	0.126744
	covariance matrix	0.000527	- 0.000029	- 0.000064	0.012360	0.000537	- 0.000064	- 0.000058	0.011377
		- 0.000029	0.000493	- 0.000110	0.021405	- 0.000064	0.000512	- 0.000109	0.020593
		- 0.000064	- 0.000110	0.000034	- 0.006623	- 0.000058	- 0.000109	0.000033	- 0.006323
		0.012360	0.021405	- 0.006623	1.508948	0.011377	0.020593	- 0.006323	1.420589